nature physics

SUPPLEMENTARY INFORMATION

https://doi.org/10.1038/s41567-018-0233-6

In the format provided by the authors and unedited.

Enhanced high-harmonic generation from an all-dielectric metasurface

Hanzhe Liu[1,2*], Cheng Guo[3,4], Giulio Vampa[1], Jingyuan Linda Zhang[3,4], Tomas Sarmiento[4,5], Meng Xiao[4], Philip H. Bucksbaum[1,2,3,6], Jelena Vučković[3,4,5], Shanhui Fan[3,4,5] and David A. Reis[1,3,6*]

[1]Stanford PULSE Institute, SLAC National Accelerator Laboratory, Menlo Park, CA, USA. [2]Department of Physics, Stanford University, Stanford, CA, USA. [3]Department of Applied Physics, Stanford University, Stanford, CA, USA. [4]E. L. Ginzton Laboratory, Stanford University, Stanford, CA, USA. [5]Department of Electrical Engineering, Stanford University, Stanford, CA, USA. [6]Department of Photon Science, Stanford University, Stanford, CA, USA. *e-mail: hanzhe@stanford.edu; dreis@stanford.edu

Supplementary Information

Enhanced High-Harmonic Generation from an All-Dielectric Metasurface

Hanzhe Liu[1,2], Cheng Guo[3,4], Giulio Vampa[1], Jingyuan Linda Zhang[3,4], Tomas Sarmiento[4,5], Meng Xiao[4], Philip H. Bucksbaum[1,2,3,6], Jelena Vučković[3,4,5], Shanhui Fan[3,4,5] and David A. Reis[1,3,6]

[1]Stanford PULSE Institute, SLAC National Accelerator Laboratory, Menlo Park, California, 94025, USA

[2]Department of Physics, Stanford University, Stanford, California, 94305, USA

[3]Department of Applied Physics, Stanford University, Stanford, California, 94305, USA

[4]E. L. Ginzton Laboratory, Stanford University, Stanford, California 94305, USA

[5]Department of Electrical Engineering, Stanford University, Stanford, California 94305, USA

[6]Department of Photon Science, Stanford University, Stanford, California 94305, USA

Resonant frequencies extraction

We extract the central resonant frequencies of the collective bar mode and disk mode from the simulated transmission spectrum using a Fano model. The fitting method is identical to the one used in Ref.[1,2].

To determine the central resonant frequency of the broadband bar mode, we utilize the fact that the 'dark' disk mode will not be efficiently excited due to destructive interference when the gap between the disk and the two adjacent bars are exactly equal[1]. For convenience, we refer to this configuration as 'symmetric', and the configuration studied in the main text as 'asymmetric'. Figure S1**a** shows the simulated transmission spectra of the 'symmetric' and

'asymmetric' device, which differ only in the frequency region around the EIT peak but overlap well for frequencies away from the EIT peak. As expected, the transmission for the 'symmetric' device only exhibits one Fano-like resonance due to the excitation of the 'bright' bar mode. In Fig. S1**b** we fit the transmission for the 'symmetric' device to a Fano line shape given by $T(\omega) = \left|a_1 + ia_2 + \frac{b}{\omega - \omega_0 + i\gamma}\right|^2$, where a_1, a_2 and b are real constants, ω_0 is the central resonant frequency and γ is the resonance linewidth. The fit is almost perfect and the central resonant frequency for the bar mode is determined as $\omega_{0,bar} = 8.127 \times 10^{14}\ rad/s$, or equivalently, the central resonant wavelength $\lambda_{0,bar} = 2.318\ \mu m$.

To determine the central resonant frequency of the narrowband disk mode, we perform the Fano fitting to the transmission for the 'asymmetric' device. As the lineshape for the dark mode is much narrower than the bright mode, we use the same single Fano resonance model used above. This fit model is approximate since it does not include the fit of the background resonance induced by the bright mode; however, it is accurate enough for the extraction of the resonant frequency of the dark mode, as shown in Ref.[2]. The fit is performed over a frequency range from $8.105 \times 10^{14}\ rad/s$ to $8.143 \times 10^{14}\ rad/s$, and is fairly good in this frequency range as shown in Fig. S1**c**. The central resonant frequency for the disk mode is determined as $\omega_{0,disk} = 8.117 \times 10^{14}\ rad/s$, corresponding to the central resonant wavelength $\lambda_{0,disk} = 2.321\ \mu m$.

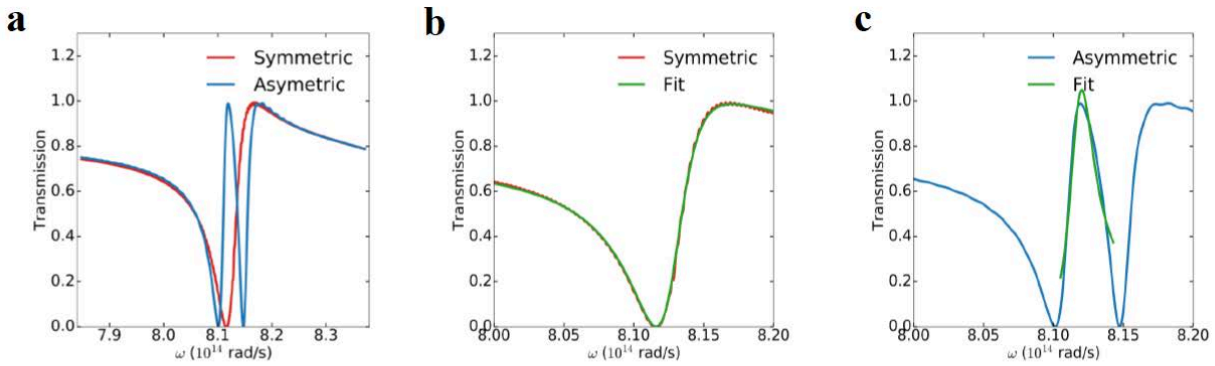

Figure S1 | Extraction of resonant frequencies. a, Simulated transmission spectra of the metasurface for both 'asymmetric' and 'symmetric' configurations. **b**, Fit of the bar mode with a Fano-shape resonance. **c**, Fit of the disk mode in the vicinity of the EIT peak in the 'asymmetric' configuration.

The role of device damage in the observed saturation behavior

In the main text, we report a gradual saturation of the high harmonic yield as a function of increasing intensity. When the excitation intensity is subsequently decreased, the measured harmonic yield is reduced from its initial value, indicating progressive and permanent damage of the metasurface. This contributes to the saturation behavior seen in Fig. 3 of the main text, on top of any dynamic field-induced saturation in the harmonic generation process.

Fig. S2 shows example SEM images various locations on the metasurface without (S2**a**) and after illumination (S2**b** and S2**c**). As observed in Fig. S2**b**, after moderate pump intensity ~0.1 TW/cm^2, only disks in the metasurface are damaged. This is consistent with the FDTD simulation result shown in Fig. 1**f** in the main text that the excitation field is peaked at the center of the disk. Each disk in our device exhibit slightly different field enhancement inside, a result of

small fluctuation in shape introduced by the imperfection of the nanofabrication process. Disks with higher field enhancement are more easily to damage at a lower intensity, forming a random distribution of damaged structures as observed in Fig. S2**b**. As the intensity is increased, more structures, including both disks and bars, start to damage as shown in Fig. S2**c** taken after exposure at an intensity of ~0.28 TW/cm^2.

The observed saturation behavior in Fig. 3 in the manuscript can then be understood at least in part as follows. At a fixed high excitation intensity, a fraction of the structures that appear randomly located at the laser focus will be damaged. As the pump intensity is increased, the balance between the total reduced number of undamaged structures and the enhanced emission efficiency from individual structures could, in principal, lead to the observed saturation in Fig. 3. Since part of the structures are already damaged, the measured HHG yield in Fig. 3 does not trace back when the pump intensity is decreased after reaching the maximum intensity.

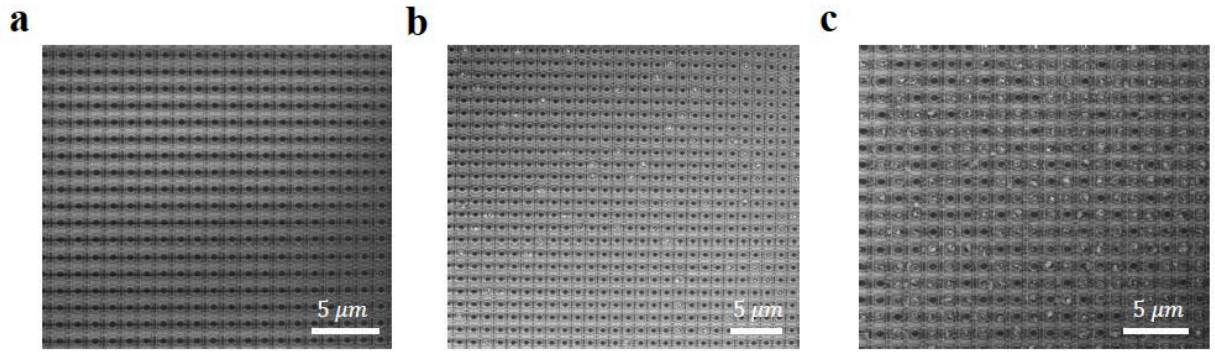

Figure S2 | SEM images of the metasurface after laser exposure. a, undamaged metasurface. **b**, SEM image of the metasurface after moderate laser excitation ~0.1 TW/cm^2. Only a small portion of disks are

damaged. The damage pattern in the field of view is randomly distributed. c, SEM image of the damaged metasurface after exposed under an intensity of 0.28 TW/cm^2.

Reference:

1. Yang, Y., Kravchenko, I. I., Briggs, D. P. & Valentine, J. All-dielectric metasurface analogue of electromagnetically induced transparency. *Nat. Commun.* **5,** 5753 (2014).
2. Wu, C. *et al.* Spectrally selective chiral silicon metasurfaces based on infrared Fano resonances. *Nat. Commun.* **5,** 1–9 (2014).